Possible Global Magneto-Fluid Structure of the Stellar Convection Zone

Sanae I. ITOH

Research Institute for Applied Mechanics, Kyushu University, Kasuga, Fukuoka 816-8580

s-iitoh@riam.kyushu-u.ac.jp

Kimitaka ITOH

National Institute for Fusion Science, Toki, Gifu 509-5292

itoh@nifs.ac.jp

Patrick H. DIAMOND

Department of Physics, University of California San Diego, La Jolla, CA 92093-0319, U.S.A.

phd@physics.ucsd.edu

and

Akira YOSHIZAWA

National Institute for Fusion Science, Toki, Gifu 509-5292

ay-tsch@mbg.nifty.com

Abstract

Structures of the magnetic field and velocity in stars are discussed based on the mean field MHD equations. A special case is presented, where the solution is constructed by the Beltrami solution in the stellar convection zone with the symmetry in the azimuthal direction. Magnetic field lines form concentric toroidal magnetic surfaces. The cross-helicity dynamo mechanism induces a mean flow of plasmas. The structure of this driven flow is also shown to constitute toroidal surfaces. Considering the symmetry and the relation of this toroidal magnetic structure with the polarity, it is shown that the latitudinal component of this flow is pole-ward in the northern as well as southern hemispheres. This gives an insight into the role of the magnetic field for the meridional flow.

Key words: magnetic field: MHD — plasmas: magnetofluid torus — stars: convection zone — stars: meridional flow — turbulence: cross-helicity dynamo

1. Introduction

The magnetic and flow structures in stars have attracted attention. The magnetic structure and the flow structure in the convection zone (e.g., the solar convection zone) have been subject to intensive studies in relation to dynamo problems. (See, e.g., reviews Moffat 1978; Krause, Raedler 1980; Priest 1982; Parker 1993; Lang 2001; Shibahashi 2002; Diamond, et al. 2004; Yoshizawa et al. 2004.) The effect of the magnetic field on the flow is reconsidered, as was recently summarized (Shibahashi 2004), and requires further studies. Besides the conventional turbulent dynamo mechanisms, like alpha- and beta-dynamo (i.e., the turbulent helicity effect and turbulent resistivity), a turbulent cross-helicity dynamo has been predicted (Yoshizawa 1990; Blackman, Chou 1997). In this mechanism, the electromotive force is driven in proportion to the fluid vorticity. The counterpart of this process appears in the equation of the fluid dynamics. That is, a turbulence force, which is in proportion to the inhomogeneous mean magnetic field, appears when the turbulent cross-helicity does not vanish.

This mechanism is applied to astrophysical plasmas. One example is given in the problem of generating toroidal and poloidal magnetic fields and a reversal of the magnetic field. The other example considers the relationship between the magnetic activity (as is revealed as sun spots and star spots) and the perturbed oscillations. In addition to the Lorenz force model (Yoshimura 1981), the cross-helicity dynamo mechanism has been discussed (Itoh et al. 2005). Studies have shown that the cross-helicity dynamo mechanism has important influences on the evolution of the magnetic field and flow in astrophysical objects.

This article reports on possible magneto-fluid structures of the convection zone of stars in the presence of a strong cross-helicity dynamo process (Yoshizawa et al. 2000; Blackman 2000). Possible stationary structures are discussed, but dynamics are not treated. Based on the turbulent electromotive force, a toroidal structure of the magnetic field is predicted to exist. Then, the plasma flow driven by this magnetic field through the cross-helicity dynamo mechanism is considered. It is shown that the meridional flow can be induced by the toroidal magnetic structures. When the magnetic field satisfies the polarity rule (i.e., the symmetry property across the equatorial plane), the meridional flow driven by the cross-helicity dynamo mechanism can direct pole-ward both in the northern and southern hemispheres.

In section 2, basic equations to start with are shown, together with the imposed boundary conditions. Assumptions are introduced. Then, the formal solutions of the magnetic field and the flow structures are obtained in a spherical geometry. In section 3, the solutions are shown and the structures of the magnetic field and flow velocity are illustrated. Implications of the solution are discussed. In the final section, a summary and discussions are given.

2. Basic Equations

One way to explain the meridional flow is based on the Eddington–Sweet mechanism (Sweet 1950), which is caused by the temperature gradient of the latitudinal direction. (Such a case is discussed in appendix 1.) In this article we consider the role of coupling between the magnetic field and the flow. In order to study this mechanism, we choose the limit, for the transparency of the argument, where the baroclinicity is ignored and the thermal wind balance holds. The basic equations we start with are the mean-field MHD equations in the following (Yoshizawa et al. 2003):

$$\frac{\partial u_i}{\partial t} + \frac{\partial}{\partial x_j} u_i u_j = -\frac{\partial}{\partial x_i}\left(p + \left\langle \frac{B'^2}{2}\right\rangle\right) + 2(\boldsymbol{u} \times \boldsymbol{\omega}_{\mathrm{F}})_i$$

$$+ (\boldsymbol{J} \times \boldsymbol{B})_i + \frac{\partial}{\partial x_j}(-R_{ij}) + \nu\nabla^2 u_i, \quad (1)$$

in the frame rotating with angular velocity $\boldsymbol{\omega}_{\mathrm{F}}$, and the induction equation,

$$\frac{\partial \boldsymbol{B}}{\partial t} = \nabla \times (\boldsymbol{u} \times \boldsymbol{B} + \boldsymbol{E}_{\mathrm{T}}) + \eta\nabla^2\boldsymbol{B}, \quad (2)$$

where the turbulent electromotive force and the Reynolds stress are given as

$$\boldsymbol{E}_{\mathrm{T}} \equiv \langle \boldsymbol{u}' \times \boldsymbol{B}'\rangle = \alpha\boldsymbol{B} - \beta\boldsymbol{J} + \gamma(\boldsymbol{\omega} + 2\boldsymbol{\omega}_{\mathrm{F}}), \quad (3)$$

$$R_{ij} \equiv \langle u_i' u_j' - B_i' B_j'\rangle$$

$$= \frac{1}{3}\langle u'^2 - B'^2\rangle\delta_{ij} - \nu_{\mathrm{T}}\left(\frac{\partial u_j}{\partial x_i} + \frac{\partial u_i}{\partial x_j}\right)$$

$$+ \nu_{\mathrm{M}}\left(\frac{\partial B_j}{\partial x_i} + \frac{\partial B_i}{\partial x_j}\right). \quad (4)$$

Here, equation (1) is the global flow equation in the presence of microscopic MHD turbulence, $\boldsymbol{u}$ is the relative velocity in the rotation frame, p is the pressure per unit mass with effects of microscopic pressure fluctuation included, $\boldsymbol{B}$ is the magnetic field, $\boldsymbol{J}$ ($= \nabla \times \boldsymbol{B}$) is the electric current, ν is the molecular viscosity, and η is the magnetic diffusivity. These equations are given in the Alfvén unit, where the magnetic field is normalized to $\sqrt{\mu_0\rho}$, and is measured in $\mathrm{m\,s^{-1}}$ (ρ is the mass density). Quantities with prime (ʹ) indicate the fluctuating elements. Turbulent transport coefficients, which generate the mean magnetic field, are defined as $\alpha = C_\alpha\langle -\boldsymbol{u}' \cdot \nabla \times \boldsymbol{u}' + \boldsymbol{B}' \cdot \nabla \times \boldsymbol{B}'\rangle\tau_{\mathrm{c}}$ and $\gamma = C_\gamma\langle \boldsymbol{u}' \cdot \boldsymbol{B}'\rangle\tau_{\mathrm{c}}$, where τ_{c} is the correlation time of the turbulence. The magnetic diffusion coefficient, β, is also expressed in terms of the spectrum of the velocity and the magnetic field fluctuations. In the dynamics of the flow, the turbulent viscosity, ν_{T}, and the drive by the inhomogeneity of magnetic field, the coefficient for which is given by ν_{M}, appear. Introducing the property of the 3D MHD turbulence, β can be expressed in terms of the kinematic magnetic diffusivity, $\beta = C_\beta\langle \boldsymbol{u}'^2\rangle\tau_{\mathrm{c}}$ (Diamond et al. 2004; Vainshtein, Kitchatinov 1983). Some details concerning the dynamo coefficient, which are used here, are given in Yoshizawa et al. (2004), and a brief derivation is given in appendix 2. Noting that β and ν_{T} are induced by the fluctuation energy intensity, while γ and ν_{M}

are caused by the cross-helicity of the MHD perturbations, an evaluation has been given,

$$\frac{\nu_{\mathrm{M}}}{\nu_{\mathrm{T}}} \simeq \frac{\gamma}{\beta} \quad (5)$$

[see: Yoshizawa et al. (2004). Note that other modeling may provide a relation with a different magnitude of the ratio C_{r}, e.g., $\nu_{\mathrm{M}}/\nu_{\mathrm{T}} \simeq C_{\mathrm{r}}\gamma/\beta$. Nevertheless, the difference in the ratio C_{r} does not cause a qualitative change in the conclusion of this analysis.] Equation (3) illustrates the conventional α-dynamo (helicity dynamo), β-dynamo (turbulent resistivity), and the cross-helicity dynamo. Note that the symbol γ indicates the cross-helicity dynamo in this article, and does not denote the anti-symmetric part of α, which is used in, e.g., Moffat (1978). The gradient of the mass-weighted pressure appears in equation (1) as a total derivative, ∇p. The mean-field dynamical equations have been studied in rotating system (e.g., Rüdiger, Kitchatinov 1990), and this model of the mean-field equations is consistent with the line of thought in (Rüdiger, Kitchatinov 1990). We note here simplifications of equations (3) and (4), where dynamo coefficients $(\alpha, \gamma, \ldots)$ are modeled as scalar (or pseudo-scalar) quantities. In principle, they are tensors, and the approximation to employ scalar (pseudo-scalar) coefficients has a limitation (e.g., Rüdiger, Hollerbach 2005). Nevertheless, such a simplified model has also been proved to be relevant for understanding the qualitative feature of the structure formation in strong MHD turbulence, as demonstrated by Taylor and other researchers (Taylor 1986). In the first step to understand the magnetofluid structure, driven by the cross-helicity dynamo mechanism, we choose this simplified, but fruitful, model.

In order to obtain a possible solution with a global structure, we consider the case where the turbulent viscosity is large enough compared with the molecular viscosity, and the resistive diffusion of the magnetic field is neglected. For transparency of the argument, the stationary solution, $\partial\boldsymbol{B}/\partial t = 0$, for the case of constant dynamo coefficients of (α, β, γ) is considered. Under this circumstance, substitution of equation (3) into equation (2) gives

$$\frac{\partial \boldsymbol{B}}{\partial t} = \nabla \times [\boldsymbol{u} \times \boldsymbol{B} + \alpha\boldsymbol{B} - \beta\boldsymbol{J} + \gamma(\boldsymbol{\omega} + 2\boldsymbol{\omega}_{\mathrm{F}})]. \quad (6)$$

We are interested in a special case of $\boldsymbol{u} \parallel \boldsymbol{B}$, and search for the solution employing the approximation of dropping $\boldsymbol{u} \times \boldsymbol{B}$. The velocity fields are separated into two categories. The former is the flow velocity, $\boldsymbol{u}_0$, which exists without induction by the magnetic field. The other is the response of the flow velocity, $\boldsymbol{u}$, owing to the appearance of the dynamo magnetic field. In this article we are interested in and study the latter flow. The quasi-stationary sate of $\boldsymbol{B}$ may occur through the condition

$$\boldsymbol{J} = \frac{1}{\beta}[\alpha\boldsymbol{B} + \gamma(\boldsymbol{\omega} + 2\boldsymbol{\omega}_{\mathrm{F}})]. \quad (7)$$

We substitute equation (7) into equation (1). We take the curl of the resulting equation, and have the equation of the velocity that is driven by the magnetic field, with the help of equation (5), as

$$\frac{\partial \boldsymbol{\omega}}{\partial t} = \nabla \times \left[2\left(\boldsymbol{u} - \frac{\gamma}{\beta}\boldsymbol{B}\right) \times \boldsymbol{\omega}_{\mathrm{F}} + \nu_{\mathrm{T}}\nabla^2\left(\boldsymbol{u} - \frac{\gamma}{\beta}\boldsymbol{B}\right)\right]. \quad (8)$$

The source of the torque $\nu_T \nabla^2 (\gamma/\beta) \boldsymbol{B}$ in equation (8) is the counterpart of the γ-related term in the right-hand side (RHS) of equation (6). (Note that other type of solutions, in which $\boldsymbol{u} \perp \boldsymbol{B}$-components, are also able to exist. We focus here on special solutions of $\boldsymbol{u} \parallel \boldsymbol{B}$. The structure obtained here shows analytic insight into the problem discussed later in this article.) It has been well known that the turbulent transport coefficient, α, is quenched, compared with an evaluation based on a kinematic evaluation, by the generated mean magnetic field (Diamond et al. 2004). It is possible that the turbulent viscosity, ν_T, is also quenched by the generated mean magnetic field. In this article, we assume that the quenching rate of ν_T (for given generated mean magnetic field) is not stronger than the quenching of α.

Under these assumptions and conditions, solutions that satisfy

$$\alpha \boldsymbol{B} - \beta \boldsymbol{J} + \gamma(\boldsymbol{\omega} + 2\boldsymbol{\omega}_F) = 0 \tag{9}$$

and

$$\boldsymbol{u} = \frac{\gamma}{\beta} \boldsymbol{B} \tag{10}$$

are searched. [In deducing equation (9) from equation (6) for stationary and axisymmetric solutions, the right hand side of equation (9) has a freedom of the gauge field, $\nabla \phi$, ϕ being such as the electrostatic potential. The effect of the electrostatic potential in the stellar plasmas could be important, but is out of the scope of this article. Thus, we employ equation (9).] From equations (9), (10), and the relation, $\boldsymbol{J} = \nabla \times \boldsymbol{B}$, we have

$$\nabla \times \boldsymbol{B} - \frac{\alpha}{\lambda_u \beta} \boldsymbol{B} = \frac{2\gamma}{\lambda_u \beta} \boldsymbol{\omega}_F, \tag{11}$$

where

$$\lambda_u \boldsymbol{B} = \boldsymbol{B} - \frac{\gamma}{\beta} \boldsymbol{u} = \left[1 - \left(\frac{\gamma}{\beta} \right)^2 \right] \boldsymbol{B}. \tag{12}$$

The homogeneous solution of equations (11) and (12) leads to the Beltrami solution of $(\boldsymbol{B}, \boldsymbol{J}, \boldsymbol{u}, \boldsymbol{\omega})$,

$$\nabla \times \begin{pmatrix} \boldsymbol{B} \\ \boldsymbol{J} \\ \boldsymbol{u} \\ \boldsymbol{\omega} \end{pmatrix} = \frac{\alpha}{\lambda_u \beta} \begin{pmatrix} \boldsymbol{B} \\ \boldsymbol{J} \\ \boldsymbol{u} \\ \boldsymbol{\omega} \end{pmatrix}. \tag{13}$$

Inhomogeneous solutions are obtained accordingly, and the solution of our interest is shown after introducing spherical coordinates.

In order to obtain typical structures, we introduce spherical coordinates (r, θ, ζ), where $\theta = 0$ corresponds to the rotation axis, and the coordinates are shown in figure 1. The symmetry is imposed on the ζ-direction (toroidal direction, or longitudinal direction) $\partial/\partial \zeta = 0$.

In the beginning, we seek homogeneous solutions. Taking the rotation of equation (11), we readily obtain

$$\nabla^2 \boldsymbol{B} + \left(\frac{\alpha}{\lambda_u \beta} \right)^2 \boldsymbol{B} = 0. \tag{14}$$

The toroidal (longitudinal) component of the magnetic field, B_ζ, satisfies

z

ζ

r

r_c

θ

r_0

0   equatorial plane
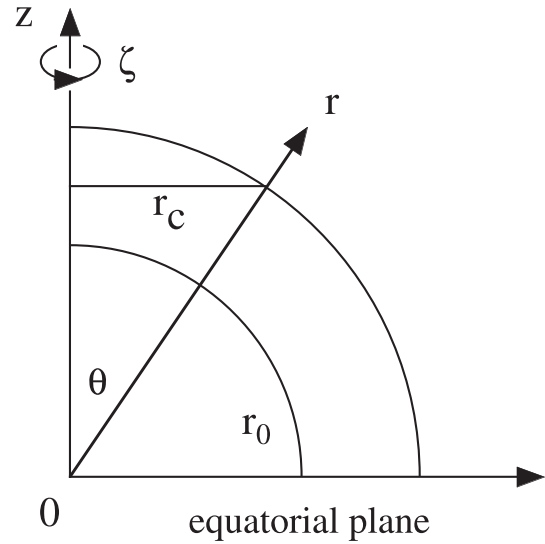
Fig. 1. Spherical coordinates (r, θ, ζ).

$$\frac{1}{r^2} \frac{\partial}{\partial r} \left(r^2 \frac{\partial}{\partial r} B_\zeta \right) + \frac{1}{r^2 \sin\theta} \frac{\partial}{\partial \theta} \left(\sin\theta \frac{\partial}{\partial \theta} B_\zeta \right)$$
$$- \frac{1}{r^2 \sin^2\theta} B_\zeta + \left(\frac{\alpha}{\lambda_u \beta} \right)^2 B_\zeta = 0. \tag{15}$$

General solutions for B_ζ and B_θ are formally written in terms of the n-th order spherical Bessel functions (j_n and n_n) and the associated Legendre function of $P_n^{(m)}$ as

$$B_\zeta(r, \theta) = \sum_n [a_n j_n(y) + b_n n_n(y)] P_n^{(1)}(\cos\theta), \tag{16}$$

$$B_\theta(r, \theta) = -\sum_n \left\{ a_n \left[\frac{n+1}{y} j_n(y) - j_{n+1}(y) \right] \right.$$
$$\left. + b_n \left[\frac{n+1}{y} n_n(y) - n_{n+1}(y) \right] \right\} P_n^{(1)}(\cos\theta), \tag{17}$$

$$B_r(r, \theta) = \sum_n [a_n j_n(y) + b_n n_n(y)] y^{-1}$$
$$\times \left[\frac{2\cos\theta}{\sin\theta} P_n^{(1)}(\cos\theta) - P_n^{(2)}(\cos\theta) \right], \tag{18}$$

where

$$y = \frac{\alpha}{\lambda_u \beta} r. \tag{19}$$

The flow velocities, (u_r, u_θ, u_ζ), are also given by using equation (10) and equations (16)–(19). Thorough description of the representation in terms of spherical harmonics has been discussed in, e.g., Yoshimura 1972.)

An inhomogeneous solution of $\boldsymbol{B}$, namely, the toroidal field $B_{\zeta 0} \hat{\zeta}$, comes from rigid rotation, and is given in the form of a toroidal (longitudinal) magnetic field by Yoshizawa et al. (2000). Taking into account the screening effect, λ_u, here, a form is given as

$$B_{\zeta 0} = \frac{2\gamma}{\lambda_u \beta} \omega_F r \sin\theta, \tag{20}$$

and $u_{\zeta 0}$ is also obtained as

$$u_{\zeta 0} = (\gamma/\beta)B_{\zeta 0}. \tag{21}$$

The total fields are given as $\boldsymbol{B}_{\text{tot}} = \boldsymbol{B} + B_{\zeta 0}\hat{\zeta}$ and $\boldsymbol{u}_{\text{tot}} = \boldsymbol{u} + u_{\zeta 0}\hat{\zeta}$, respectively.

3. Possible Solutions for Toroidal Structure

Let us analyze possible magnetic and associated flow structures based on the solutions in section 2. Here, plausible boundary conditions as well as the constraints are given, and the solutions are illustrated.

3.1. Magnetic Torus

3.1.1. Toroidal structure

We here choose the lower order structure of poloidal harmonics n ($n \geq 1$), which is even from the up-down symmetry. (That is, the form of toroidal structure is symmetric with respect to the equatorial plane. The up-down symmetry of the sign of the magnetic field is discussed later.) The boundary condition in radius is given at the lower and upper boundaries, $r = r_{\text{in}}$ and $r = r_{\text{out}}$. On these surfaces, the radial magnetic field vanishes. (Note that this condition is chosen for the case that the Taylor number is not very high. In the limit of the large Taylor number, structures are expected to become homogeneous in the z-direction. If this is the case, the boundary condition is given in terms of the cylindrical radius, r_{c}, in figure 1. The solution, which is regular at the center, $r = 0$, is discussed in appendix 3.)

In terms of the variable y of equation (19), the boundary conditions are given at $y_{\text{in}} = \alpha/(\lambda_u \beta)r_{\text{in}}$ and $y_{\text{out}} = \alpha/(\lambda_u \beta)r_{\text{out}}$. The condition $B_\zeta(r, \theta) = 0$ at $r = r_{\text{in}}$ and $r = r_{\text{out}}$ yields

$$j_n(y_{\text{in}})n_n(y_{\text{out}}) - j_n(y_{\text{out}})n_n(y_{\text{in}}) = 0 \tag{22}$$

and

$$\frac{y_{\text{out}}}{y_{\text{in}}} = \frac{r_{\text{out}}}{r_{\text{in}}}. \tag{23}$$

These eigenvalue equations (22) and (23) provide a series of solutions, even if the poloidal mode number, n, is chosen. (For instance, $y_{\text{out}} = 3.46\pi$, 6.73π, 10.04π, ..., for $n = 2$ and $r_{\text{in}}/r_{\text{out}} = 0.7$.) The eigenvalue is chosen here as the minimum eigenvalue which satisfies equations (22) and (23). The plausibility argument for this is given later in conjunction with quenching of the dynamo coefficients (Diamond et al. 2004). [This is also related to the consideration of minimum principle. Under the circumstance of the fully developed MHD turbulence, the final state is conjectured as the minimum energy state for a given helicity: Taylor state (Taylor 1986). If this is so, the radial node numbers tend to decrease. At this moment, it is not clear whether the final state is completely free from other constraints. For instance, if the Taylor number is high, then the constraints of the Taylor–Proudman theorem may prohibit access to the Taylor state. Thus, we do not require the minimum principle of magnetic energy for given magnetic helicity, but accept the smallest eigenvalue from equations (22) and (23).] Once the eigenvalue ($y_{\text{in}}, y_{\text{out}}$) is obtained, the magnetic field solution is given putting $b_n = -j_n(y_{\text{in}})n_n^{-1}(y_{\text{in}})a_n$ into equations (16)–(18) as

$$B_\zeta(r, \theta) = a_n \left[j_n(y) - \frac{j_n(y_{\text{in}})}{n_n(y_{\text{in}})}n_n(y) \right] P_n^{(1)}(\cos\theta)$$
$$+ \frac{\gamma}{\lambda_u \beta}\omega_F r \sin\theta, \tag{24}$$

$$B_\theta(r, \theta) = -a_n \left\{ \frac{n+1}{y}j_n(y) - j_{n+1}(y) \right.$$
$$\left. - \frac{j_n(y_{\text{in}})}{n_n(y_{\text{in}})}\left[\frac{n+1}{y}n_n(y) - n_{n+1}(y) \right] \right\} P_n^{(1)}(\cos\theta), \tag{25}$$

$$B_r(r, \theta) = a_n \left[\frac{j_n(y)}{y} - \frac{j_n(y_{\text{in}})n_n(y)}{y\,n_n(y_{\text{in}})} \right]$$
$$\times \left[\frac{2\cos\theta}{\sin\theta}P_n^{(1)}(\cos\theta) - P_n^{(2)}(\cos\theta) \right]. \tag{26}$$

Now the coefficient a_n represents the magnitude of the magnetic field of the homogeneous solution.

The resulting equations (24)–(26) show that the magnetic field lines constitute concentric toroidal surfaces. The radial and poloidal magnetic field is expressed as

$$\begin{pmatrix} B_r \\ B_\theta \end{pmatrix} = \begin{pmatrix} \dfrac{1}{r^2 \sin\theta}\dfrac{\partial}{\partial\theta}\psi \\ -\dfrac{1}{r \sin\theta}\dfrac{\partial}{\partial r}\psi \end{pmatrix}, \tag{27}$$

where $\psi = r\sin\theta B_{\zeta,\text{h}}\lambda_u \beta/\alpha$ and $B_{\zeta,\text{h}}$ is the longitudinal component of the homogeneous solution of the magnetic field. The radial and poloidal components of magnetic surface satisfy the relation

$$(B_r, B_\theta) \cdot \nabla_\perp \psi = 0, \tag{28}$$

where $\nabla_\perp$ represents the derivative in the radial and poloidal directions. Thus, ψ is the stream function (flux function) of the magnetic field. The contour of ψ represents the cross-section of the toroidal magnetic surface. The cross-sections of the toroidal magnetic surfaces are shown in figure 2. The lowest order number, $n = 2$, represents the solution shown in figure 2 (left), in which the toroidal structure extends from the equator to the pole, and the one magnetic axis exists in both of the northern and southern hemispheres, respectively. The solution of $n = 4$ stands for the case where the pairs of tori are sustained in both the northern and southern hemispheres (figure 2 right). Two magnetic axes appear in both hemispheres. In this case, the eigenvalue y_{out} is given as $y_{\text{out}} = 3.73\pi$, 6.88π, 10.14π, ..., for $r_{\text{in}}/r_{\text{out}} = 0.7$.

3.1.2. Magnetic field structure

We here discuss the polarity of the magnetic field. Noting the fact that the turbulent resistivity, β, is a scalar quantity, but the turbulent helicity, α, and the turbulent cross-helicity, γ, are pseudo-scalar, the ratios α/β and γ/β change their signs under the mirror transformation. Thus, we take that α/β and γ/β have the property of anti-symmetry across the equatorial plane. Equation (24) shows that B_ζ changes sign between the upper and lower hemispheres. (So is the radial component of the magnetic field.) The poloidal magnetic field (magnetic field component in the longitudinal direction) has the same sign
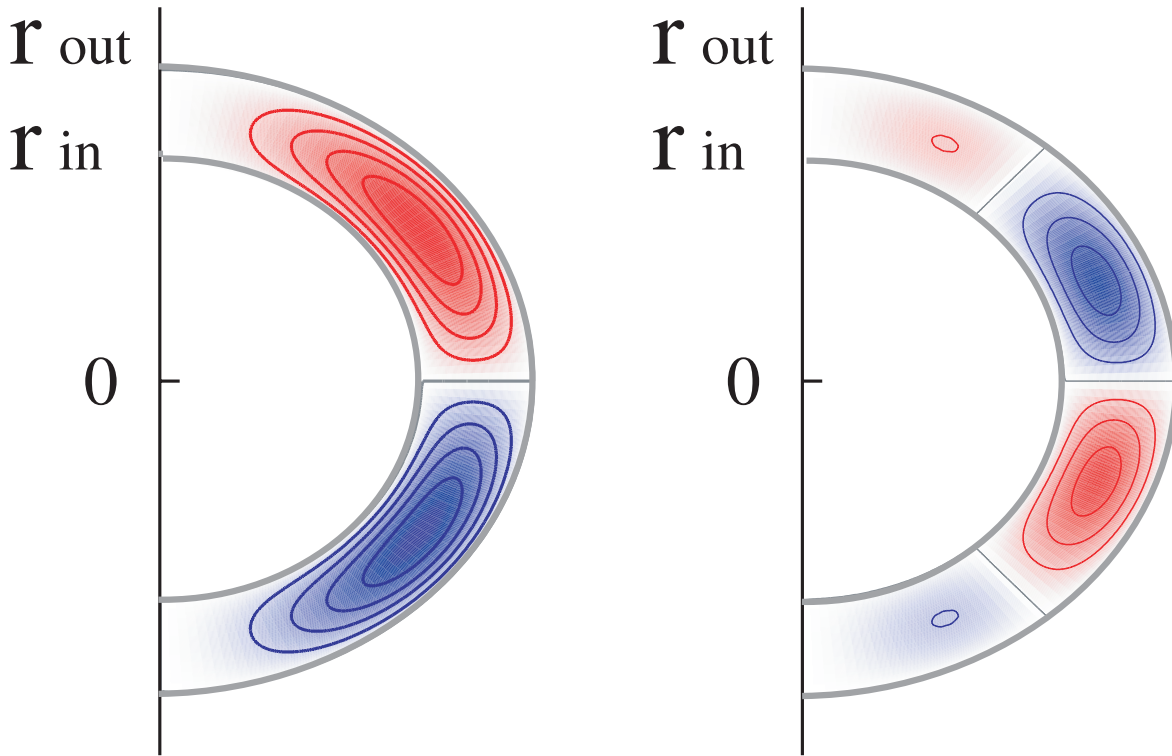
Fig. 2. Cross-sections of the toroidal magnetic structure in the convective zone. The case of $n = 2$ (left) and $n = 4$ (right).

across the equatorial plane. Figure 3 illustrates the polarity of the magnetic field on the magnetic surface. In the case of figure 3, the rotational transform of the magnetic field is chosen to be right-handed in the northern hemisphere. Then, it is left-handed in the southern hemisphere. The sign of the toroidal magnetic field is opposite, but the sign of the latitudinal magnetic field is common.

The projection of the poloidal (latitudinal) and toroidal (longitudinal) magnetic fields on the surface is illustrated in figure 4 left. This indicates that the magnetic field in the higher-latitudinal region is attributed to the second torus which has an opposite helicity in comparison with the fundamental torus in the lower latitudinal region. For instance, the toroidal magnetic field in the lower-latitudinal region of the upper hemisphere is right-handed for the case of figure 3. [The helix of magnetic field line is right-handed, i.e., B_ζ is in the same direction as $\nabla \times (B_r \hat{r} + B_\theta \hat{\theta})$.] The toroidal magnetic structure in the higher-latitudinal region is left-handed.

A pair of toroidal magnetic structure can be embedded in a hemisphere, as is illustrated in figure 2 (right). The change of helicity (i.e., right-handed in the lower-latitude torus and left-handed for the higher-latitude torus) occurs when the sign of the coefficient α is different. That is, α is positive in the lower latitudinal region and is negative in the higher latitudinal region. The difference in the sign of α is plausible owing to the geometrical consideration. The temperature gradient is perpendicular to the rotation axis in the lower latitudinal region, and is parallel to the rotation axis in the higher latitudinal region. This leads to a difference in the turbulent convection, as is discussed in Busse (1994). The dependence of the coefficient α on the poloidal angle has also been discussed in the literature, e.g.,
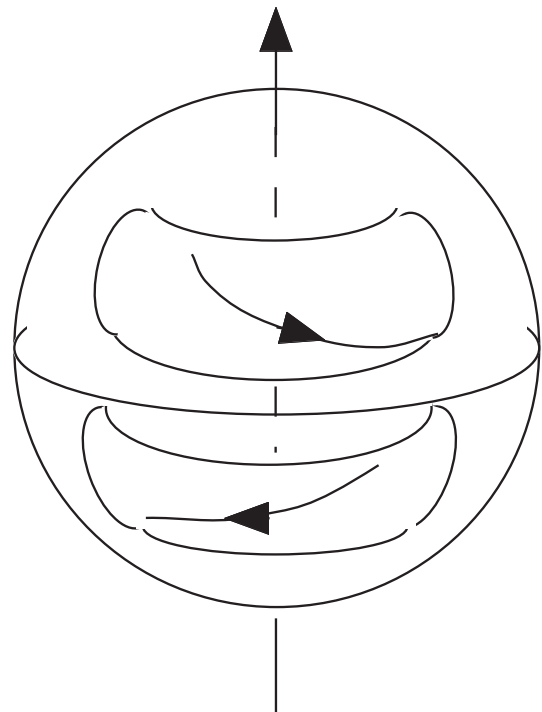
Fig. 3. Schematic view of toroidal flux surfaces: one in the northern hemisphere and the other in the southern hemisphere.

Rüdiger, Brandenburg (1995), Covas et al. (2001). Figure 4 (right) indicates the pair of torus and direction of magnetic field in the upper hemisphere corresponding to the case of figure 3.
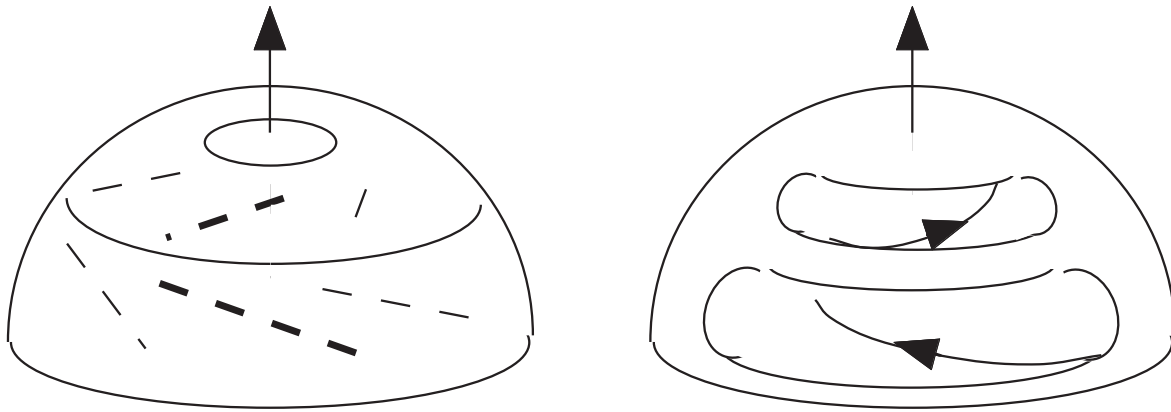
Fig. 4. Observed magnetic field direction on the surface of northern hemisphere is shown by dotted lines in the left panel. A pair of tori with opposite helicity in the northern hemisphere (right).
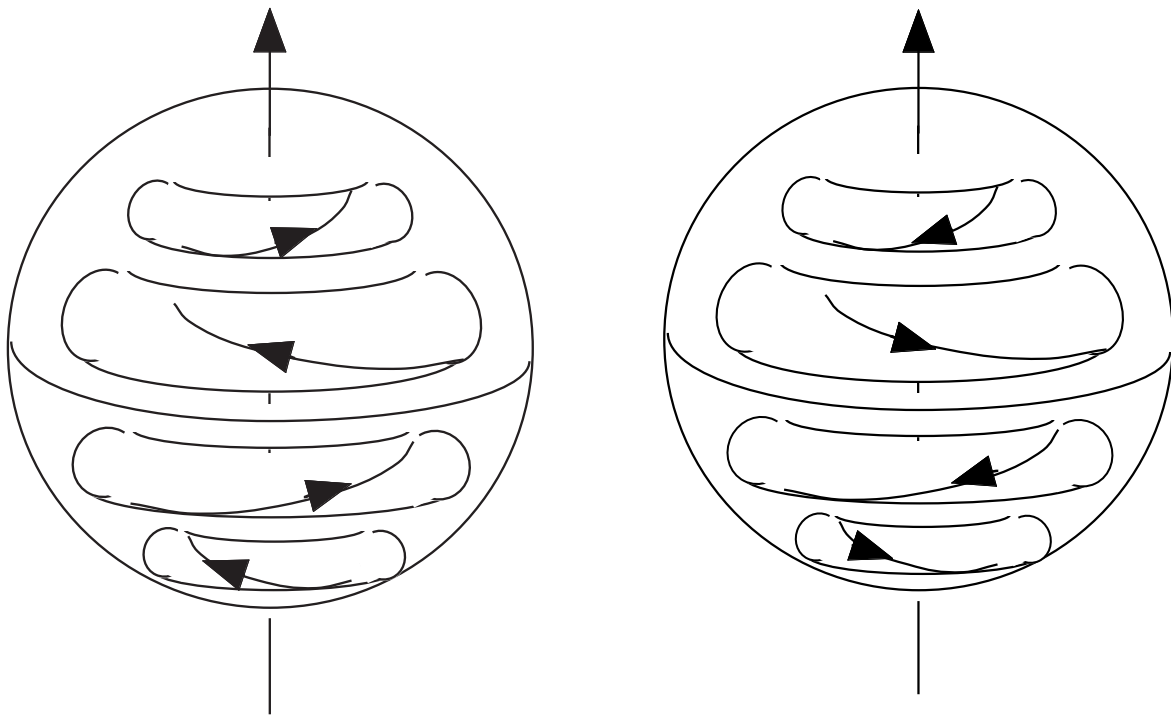
Fig. 5. Schematic drawing of the toroidal magnetic field. (a) and (b) illustrates the two phases of opposite sign of the magnetic field.

The magnetic field in the southern hemisphere has a parity relation compared with the northern hemisphere. The right (left)-handed torus is transformed into the left (right)-handed torus, respectively, as is shown in figure 5 (left).

Before closing this subsection, we note the possible quenching effect of dynamo coefficients owing to the induced magnetic field. The magnitude of the magnetic field is simultaneously determined from the global structure. Let us consider the case that the large values are given for ratios α/β and γ/β in the kinematic theory of dynamo. That is, from equation (22), a large number of radial nodes are allowed in between $r_{\rm in}$ and $r_{\rm out}$ for these values. As the generated magnetic field increases, the dynamo coefficient, α, is known to be quenched,

$$\alpha = \frac{\alpha_0}{1 + R_{\rm M} B^2 V^{-2}}, \qquad (29)$$

where α_0 is the estimate in the kinematic model, $R_{\rm M}$ is the magnetic Reynolds number, and V^2 is a characteristic mean square velocity (Diamond et al. 2004). The reduction of α indicates that the eigenvalue ($y_{\rm in}, y_{\rm out}$) takes the minimum value when the growth of the magnetic field is saturated. The eigenvalue ($y_{\rm in}, y_{\rm out}$) determines the magnitude of the magnetic field.

The coefficient β is quenched more slowly than α (Diamond et al. 2004; Gurzinov, Diamond 1994). Therefore, the ratio of the mean dynamo coefficients α/β becomes smaller when the magnitude of the mean magnetic field increases. As shown in equations (16)–(18), the scale length in the real space is in proportion to β/α; the reduction of α/β means that the scale of the generated mean field becomes larger as the magnetic field becomes stronger. Accepting this consideration, we conclude that the radial scale of the toroidal structure becomes larger as
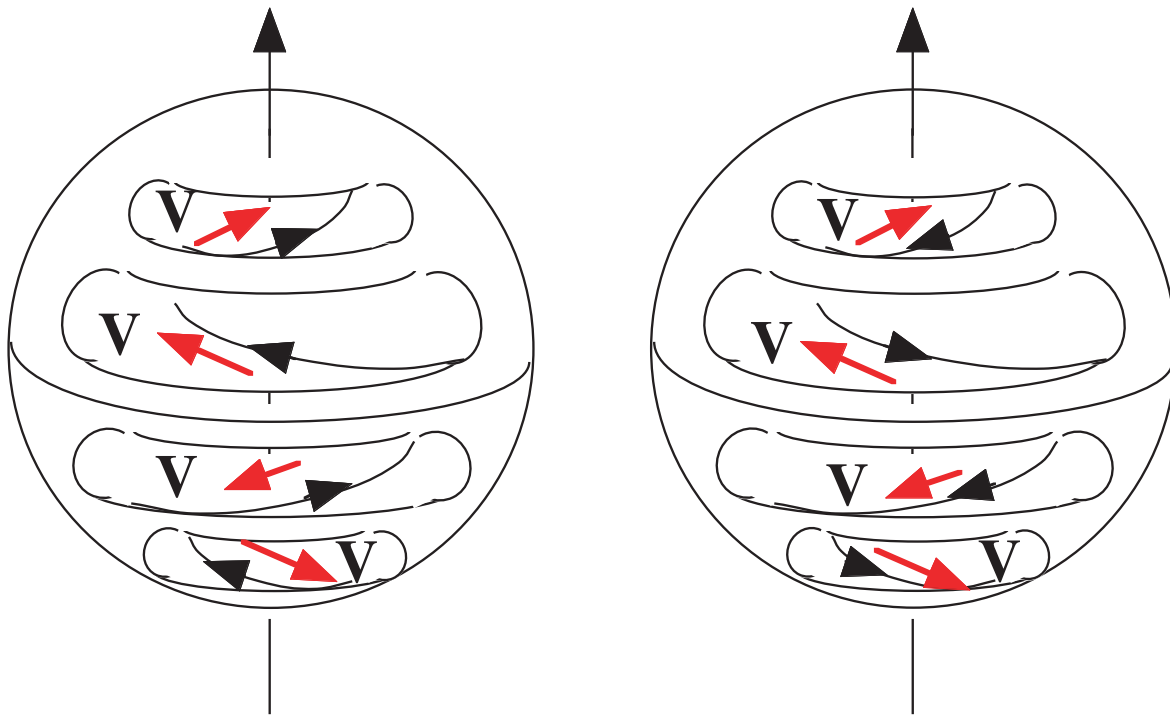
Fig. 6. Schematic drawing of the toroidal magnetic and flow structures. The black arrow indicates the magnetic field and the red arrows indicate the flow velocity. The case of the sign of the magnetic field in the case of figure 3 is shown in (left). Right panel shows the case when the sign of the magnetic field is reversed, owing to the solar magnetic cycle. In both cases, the poloidal flow which is driven by the cross-helicity dynamo is pole-ward.

the magnetic field becomes stronger. Therefore, the requirement, that the minimum of y_{in} is selected from equations (22) and (23), determines the magnitude of the magnetic field.

It is not yet concluded whether the coefficients ν_T and γ are quenched more slowly than α. The possibility of the quenching of ν_T is investigated, suggesting a slower quench than α. This issue will be discussed in a separate article (P. H. Diamond et al. 2006, in preparation).

3.2. Induced Flow with Toroidal Structure

Equation (10), $\boldsymbol{u} = (\gamma/\beta)\boldsymbol{B}$, shows that the induced flow, which is driven by the cross-helicity dynamo effect, has the same pattern as the toroidal magnetic field. The stream function of the flow constitutes the concentric toroidal surfaces.

The flow velocity, which is induced by the cross-helicity dynamo effect, is parallel to the magnetic field line. However, the direction of the flow is different from the magnetic field, as is illustrated in figure 5. The symmetry property of the magnetic field reflects the symmetry of the flow pattern. First, the relation of a pair of torus in the northern hemisphere is considered. In the main torus (lower-latitude torus), γ is chosen to be positive. In the second torus, the sign of α is reversed. In addition, the direction of the magnetic field is reversed, compared to the main torus. Therefore the coefficient γ recovers the positive sign. Thus, the coefficient γ remains positive in the northern hemisphere. This leads to the conclusion that the flow that is driven by the cross-helicity dynamo has the same direction as the magnetic field in the northern hemisphere when the magnetic field takes the sign of figure 5 (left). That is, the poloidal flow (latitudinal flow) velocity is towards the pole, but the toroidal flow (longitudinal flow)

velocity changes sign between the lower-latitude and higher-latitude regions. The cross-helicity dynamo process drives a toroidal flow. Therefore, the meridional flow closes itself on a torus. The poloidal flow is connected to the radial flow. The other property of the flow is that the direction of the radial flow changes near the latitude where the toroidal flow changes its sign.

Next, the flow velocity in the southern hemisphere is considered. According to the parity consideration, the coefficient γ has an opposite sign in the southern hemisphere. The flow velocity is indicated in figure 6 (left). The toroidal flow is symmetric across the equatorial plane, but the latitudinal flow is anti-symmetric. That is, the poloidal flow (latitudinal flow) directs to the north pole in the northern hemisphere, and to the south pole in the southern hemisphere. The meridional flows are pole-ward in both hemispheres. This solution naturally reveals the meridional flow. The direction of the magnetic field changes associated with the magnetic cycle.

The case where the sign of the magnetic field changes is illustrated in figure 6 (right). Owing to the change of the sign of the cross-helicity, the direction of the induced flow with respect to the magnetic field is reversed. As a result of this change, the flow velocity keeps the same direction. In both phases of positive and negative magnetic fields, the latitudinal component of the induced flow is pole-wards in the northern and southern hemispheres.

It is interesting to note that the plasma current, $\boldsymbol{J}$, and the flow vorticity, $\boldsymbol{\omega}$, are also parallel to the magnetic field, and the proportionality coefficients between them are $\lambda_J = \alpha/(\beta\lambda_u)$ and $\lambda_\omega = (\gamma/\beta)\lambda_J$, respectively:

$$u = \frac{\gamma}{\beta} B, \tag{30}$$

$$J = \lambda_J B, \qquad \lambda_J = \alpha/(\beta \lambda_u), \tag{31}$$

$$\omega = \lambda_\omega B, \qquad \lambda_\omega = (\gamma/\beta) \lambda_J. \tag{32}$$

All structures of B, J, u, ω are simultaneously determined from this particular mechanism. Also, the strengths are determined by the balance between α, β, and γ.

4. Summary and Discussion

In this article, the toroidal structure of the stellar magnetic field is discussed in the case that a cross-helicity dynamo process is present. The mean field dynamo equations are solved in the convection zone. A special case is presented, where the solution is constructed by the Beltrami solution in spherical coordinates with the symmetry in the longitudinal direction. Magnetic field lines are shown to form toroidal magnetic surfaces. Multiple toroidal magnetic surfaces, which are concentric, constitute a torus. A solution with two magnetic axes in the northern hemisphere (and in the solution hemisphere as well) is presented. The cross-helicity dynamo mechanism induces a mean flow of plasmas. The structure of this driven flow is also analyzed. The flow is parallel to the magnetic field line, and constitutes toroidal surfaces. Considering the parity with respect to the equatorial plane, it is shown that the latitudinal component of the flow, which is driven by the cross-helicity dynamo, is pole-ward in the northern as well as southern hemispheres. This gives one possible explanation for the meridional flow in stars. The toroidal flow (longitudinal flow), which is driven by the cross-helicity dynamo, changes its sign between the lower latitudinal region and the higher-latitudinal region. The sign of the torsional oscillation differs between the lower and higher latitudinal regions. This difference may be attributed to the dependence of toroidal flow velocity on the latitude. The other property of the predicted flow is that the direction of the radial flow changes near the latitude where the toroidal flow changes its sign. This might be examined in the near future.

The coupling between the magnetic field and flow is discussed. In the vorticity equation, the rate of the vorticity change has a term like $\nabla \times \nu_T \nabla^2 (u - \gamma B/\beta)$. One way to reduce this term is to quench the coefficient, ν_T, by the mean magnetic field. This is the Ω-quenching mechanism (Kitchatinov et al. 1994). In this article, an elimination of the difference $u - \gamma B/\beta$ is considered in the context of the cross-helicity dynamo mechanisms. Therefore, these two mechanisms are not mutually exclusive.

This way of thinking provides additional insights into solar physics. This result concerning the sign of the rotational transform may be related to the polarity rule of sunspots. Observations of sunspots have shown that: (i) the sign of the (toroidal) magnetic field is opposite between the northern and southern hemispheres. (ii) In addition, the latitudinal location of a pair of sunspots shows an inclination with respect to the latitude. That is, an eastern sunspot is at the lower latitude (i.e., closer to the equatorial plane) compared to a western sunspot. (iii) This property also holds for the southern

hemisphere. (iv) When a magnetic flux tube deviates from the toroidal magnetic surface (owing to certain instabilities, which are not specified here), the flux tube retains the memory of the rotational transform of the magnetic surface. Thus, the magnetic rotational transform naturally induces a latitudinal inclination of a pair of sunspots that appear on the solar surface. If the magnetic field changes its sign in figure 3, the geometry of inclination does not change. This gives an alternative approach to understanding the inclination of the sunspot, for which, e.g., a mechanism based on the twist by the Coriolis force has been proposed (Fan, Gong 2000). In addition, the toroidal magnetic structure occupies a large portion of the plasma, and the toroidal surfaces are in equilibrium under the gravity. (If only a thin tube is magnetized, this tube may be subject to a buoyancy motion, and is carried to the surface when the dynamo effect is weak.) As shown in section 3, the cross-helicity dynamo effect is weak on the equator, so long as the coefficient γ is anti-symmetric between the northern and southern hemispheres. The subject of this article is to consider the effects of a cross-helicity dynamo, and special solutions of $u \parallel B$ are analyzed. The result of this analysis has a limitation for phenomena on the equator. Within the model of this article, the toroidal magnetic field, B_ζ, at the surface is given by that driven by the cross-helicity dynamo. Thus, on the equator of the surface, the toroidal magnetic field vanishes. The analysis in this manuscript is based on a simple model that the coefficients (α, β, γ) do not depend on the radial position. Although this is a simplified model, it has been successfully used to study a reverse-field pinch plasma (i.e., the 'Bessel-function model' by Taylor 1986). When the inhomogeneity of the coefficients (α, β, γ) near to the surface is taken into account, the modified Bessel function model has been used. The field near surface is then modified, while the global structure is qualitatively unaltered, and can be observable near to the surface. In order to precisely explain the observation near the surface, inhomogeneity of coefficients (α, β, γ) must be taken into account. In addition, the radial transport of flow, which is driven by the cross-helicity dynamo in the convection zone, to the surface occurs. A small amount of transported angular momentum can induce flow on the surface where the mass density is very low.

The stability of the established toroidal magnetic field structure is an important issue for future studies. For instance, a small resistivity can lead to a deviation of the magnetic field from the Beltrami solution. The deviation can cause instabilities, which then tend to restore the Taylor state (Taylor 1986). The occurrence of a small-scale symmetry-breaking perturbation at the edge of the torus has been observed on laboratory plasmas, a characteristic example of which was known as edge localized modes (ELMs) (Itoh et al. 1998). Future study of such MHD instabilities of the possible toroidal magnetic structure will enrich our understanding of the origin of starspots. There are other solutions of higher order n-th poloidal eigenmode structures. Higher n-components are included in the solution if the realistic boundary condition is fulfilled. However, in this paper we focus on indicating a prototypical solution that can explain the flows towards the Arctic and Antarctic poles from the equator. More realistic solutions with precise boundary conditions are left for future work.

In brief, the essence of the argument presented here is

that turbulence cross-helicity ($\langle \tilde{v} \cdot \tilde{B} \rangle$ which appears in γ) and the mean potential vorticity ($\boldsymbol{\omega} + 2\boldsymbol{\omega}_{\mathrm{F}}$) may conspire to produce large-scale magneto-fluid Beltrami structures (i.e., field-aligned flows) in stellar convection zones. While such structures are of possible relevance to the Sun — as we discuss — they are of much greater potential interest in the context of young, rapidly rotating stars (YRRS), which have rotation periods of (at most) 1–2 days. YRRS exhibit several features that appear to be consistent with the sense of the discussion presented above. Convective YRRS exhibit both fast rotation and heightened magnetic activity, the latter increasing with rotation rate (Donati et al. 2003). YRRS exhibit 'star spot' photospheric filling factors, f, as high as 30–50%, in dramatic contrast to the case of the Sun ($f < 1\%$) (O'Neal et al. 1998). YRRS also seem to be slightly larger than expected, according to standard stellar structure theory, and to exhibit concomitantly higher photospheric temperatures (Barnes et al. 2004). Thus, the internal magnetic field of YRRS may be strong enough to directly impact the spatiotemporal structure of their convective heat-transport process. In addition, star spots are of general utility as photospheric flow 'marker particles', and the large spot filling factor should facilitate improved spatial resolution. It may thus be possible to map photospheric meridional flows in YRRS in the near future. Existing observations indicate that spots migrate toward the polar regions, again in contrast to the Sun. In summary, then, YRRS combine a large potential vorticity, convective turbulence, enhanced magnetic activity, and a non-trivial meridional flow structure, all of which are linked by the theory presented in this paper. It thus seems to be quite reasonable to speculate that such YRRS are prime candidates for manifesting the global magneto-fluid structures discussed in this paper. We will explore this speculation in future research.

Appendix 1.   Hydrodynamic Picture for Meridional Flows

The cause of meridional flow has been considered within the framework of hydrodynamics to be that the rotation frequency, ω_{F}, depends on (r, θ), $\omega_{\mathrm{F}}(r, \theta)$, not $\omega_{\mathrm{F}}(r_{\mathrm{c}})$. [Here r_{c} refers to the cylindrical radius, and $(r_{\mathrm{c}}, \zeta, z)$ constitute the cylindrical coordinates, see figure 1.] Alternatively put, $\partial \omega_{\mathrm{F}}/\partial z \neq 0$, so that the Sun is not in a Taylor–Proudman state. As a result, the equilibrium condition from equation (8) is rewritten (neglecting cross-helicity dynamo effects) as

$$\frac{\partial \boldsymbol{\omega}}{\partial t} = \nabla \times \left(-\frac{\nabla P}{\rho} + 2\boldsymbol{u} \times \boldsymbol{\omega}_{\mathrm{F}} + \nu_{\mathrm{T}} \nabla^2 \boldsymbol{u} \right), \tag{A1}$$

where ρ is the mass density, and P the total pressure.

Further simplification is used as

$$\frac{\nabla \rho}{\rho} = -\frac{\nabla \delta T}{T}, \tag{A2}$$

where δT denotes the temperature variation away from adiabatic relation. (In case of perfect adiabatic stratification, $\nabla \rho \times \nabla P = 0$ and $\nabla \rho \times \nabla T = 0$ hold.) When the hydrostatic balance in the radial direction, i.e., $\nabla P = \rho \boldsymbol{g}$, is satisfied ($\boldsymbol{g}$ is the gravitational acceleration, $\boldsymbol{g} = g\hat{r}$), the equation

$$-\frac{g}{rT}\frac{\partial \delta T}{\partial \theta} + r_{\mathrm{c}}\frac{\partial \omega_{\mathrm{F}}^2}{\partial z} - \frac{\partial}{\partial r}(\nu_{\mathrm{T}} \nabla^2 u_{\theta}) = 0 \tag{A3}$$

gives the balance relation for the poloidal flow.

Note that the relation

$$\frac{g}{rT}\frac{\partial \delta T}{\partial \theta} = r_{\mathrm{c}}\frac{\partial \omega_{\mathrm{F}}^2}{\partial z} \tag{A4}$$

has been known as the *thermal wind balance*. According to hydrodynamics, poloidal flow (meridional flow) is induced if the thermal wind balance is violated. In the Sun, the rotation frequency is observed such that Ω is larger at the equator than at high latitudes. Thus,

$$\frac{\partial \omega_{\mathrm{F}}^2}{\partial z} < 0 \tag{A5}$$

holds. The first term, $\partial \delta T/\partial \theta$, acts in the opposite direction if

$$\frac{g}{rT}\frac{\partial \delta T}{\partial \theta} < 0, \tag{A6}$$

i.e., the pole must be warmer and the equator cooler (Sweet 1950; Shibahashi 2004).

The discussion in the main text corresponds to the case of perfect adiabatic stratification, and the flow is driven by the cross-helicity dynamo process.

Appendix 2.   Cross-Helicity Dynamo

The Reynolds stress, R_{ij}, and the turbulent electromotive force, $\boldsymbol{E}_{\mathrm{M}}$, are defined by

$$R_{ij} \equiv \langle u_i' u_j' - B_i' B_j' \rangle, \quad \text{and} \quad \boldsymbol{E}_{\mathrm{M}} \equiv \langle \boldsymbol{u}' \times \boldsymbol{B}' \rangle, \tag{A7}$$

where the prime denotes the fluctuating part. Elsasser's variables, $\boldsymbol{\phi} = \boldsymbol{u} + \boldsymbol{B}$, $\boldsymbol{\psi} = \boldsymbol{u} - \boldsymbol{B}$, are also divided into the mean and fluctuating parts as

$$\boldsymbol{\phi} = \boldsymbol{\Phi} + \boldsymbol{\phi}', \qquad \boldsymbol{\psi} = \boldsymbol{\Psi} + \boldsymbol{\psi}', \tag{A8}$$

by which we define the turbulent Elsasser's stress as

$$R_{ij}^{(\mathrm{E})} = \langle \phi_i' \psi_j' \rangle. \tag{A9}$$

The turbulent electromotive force, $\boldsymbol{E}_{\mathrm{M}}$, and the Reynolds stress, R_{ij}, are rewritten in terms of $R_{ij}^{(\mathrm{E})}$ as

$$E_{\mathrm{M}i} = -\frac{1}{2}\epsilon_{ijl} R_{jl}^{(\mathrm{E})}, \tag{A10}$$

$$R_{ij} = \frac{1}{2}\left(R_{ij}^{(\mathrm{E})} + R_{ji}^{(\mathrm{E})} \right). \tag{A11}$$

The perturbations $\boldsymbol{\phi}'$ and $\boldsymbol{\psi}'$ have been solved by using the two-scale direct interaction approximation (TSDIA) method

(Yoshizawa et al. 2003). The derivation is briefly illustrated here. Separation between the microscopic scale (for fluctuations, denoted by $\boldsymbol{k}$ and τ) and macroscopic scale (for mean variables, denoted X in this appendix) is assumed, and the ratio between them is characterized by a smallness parameter, δ_S. The Fourier component of $\boldsymbol{\phi}'$ is given by the sum of the solenoidal part, $\boldsymbol{\phi}^+$, and gradient term as

$$\boldsymbol{\phi}'(\boldsymbol{k};\tau) = \boldsymbol{\phi}^+(\boldsymbol{k};\tau) + \delta_S\left[-i\frac{\boldsymbol{k}}{k^2}\frac{\partial^*\phi_i'(\boldsymbol{k};\tau)}{\partial X_i^*}\right], \quad (A12)$$

where $\boldsymbol{\phi}^+$ obeys the solenoidal condition concerning $\boldsymbol{k}$: $\boldsymbol{k}\cdot\boldsymbol{\phi}^+(\boldsymbol{k};\tau) = 0$. We expand $\boldsymbol{\phi}'$ and $\boldsymbol{\phi}^+$ in terms of δ_S as

$$\boldsymbol{\phi}'(\boldsymbol{k};\tau) = \sum_{n=0}^{\infty}\delta_S^n\boldsymbol{\phi}_n'(\boldsymbol{k};\tau), \quad \boldsymbol{\phi}^+(\boldsymbol{k};\tau) = \sum_{n=0}^{\infty}\delta_S^n\boldsymbol{\phi}_n^+(\boldsymbol{k};\tau). \ (A13)$$

Similar relations are introduced for $\boldsymbol{\psi}'$.

In order to solve the dynamical equations for the fluctuations by an iterative method, we expand them in terms of the imposed mean fields, $\boldsymbol{B}$ and $\boldsymbol{\omega}$, as

$$\boldsymbol{\phi}_0'(\boldsymbol{k};\tau) = \sum_{m=0}^{\infty}\boldsymbol{\phi}_{0m}'(\boldsymbol{k};\tau), \quad (A14)$$

with a similar expression for $\boldsymbol{\psi}_0'$.

One first solves the $O(1)$ terms in the δ_S-expansion. The leading term in the expansion (A14) obeys

$$\frac{\partial\boldsymbol{\phi}_{00i}'(\boldsymbol{k};\tau)}{\partial\tau} + \nu k^2\boldsymbol{\phi}_{00i}'(\boldsymbol{k};\tau)$$

$$- iZ_{ijl}(\boldsymbol{k})\iint\boldsymbol{\psi}_{00j}'(\boldsymbol{p};\tau)\boldsymbol{\phi}_{00l}'(\boldsymbol{q};\tau)\delta(\boldsymbol{k}-\boldsymbol{p}-\boldsymbol{q})\,d\boldsymbol{p}\,d\boldsymbol{q} = 0, \quad (A15)$$

where $Z_{ijl}(\boldsymbol{k}) = k_j D_{il}(\boldsymbol{k})$ is given by using the solenoidal operator, defined by $D_{ij}(k) = \delta_{ij} - k_i k_j k^{-2}$. We introduce the Green's function for equation (A15) as

$$\frac{\partial G_{\phi_{ij}}'(\boldsymbol{k};\tau,\tau')}{\partial\tau} + \nu k^2 G_{\phi_{ij}}'(\boldsymbol{k};\tau,\tau')$$

$$- iZ_{ilm}(\boldsymbol{k})\iint\boldsymbol{\psi}_{00l}'(\boldsymbol{p};\tau)G_{\phi_{mj}}'(\boldsymbol{q};\tau,\tau')\delta(\boldsymbol{k}-\boldsymbol{p}-\boldsymbol{q})\,d\boldsymbol{p}\,d\boldsymbol{q}$$

$$= \delta_{ij}\delta(\tau-\tau'). \quad (A16)$$

With the aid of $G_{\phi_{ij}}'$, we have the first-order terms in the expansion equation (A16) as

$$\phi_{01i}'(\boldsymbol{k};\tau) = -i(\boldsymbol{k}\cdot\boldsymbol{B})\int_{-\infty}^{\tau}G_{\phi_{ij}}'(\boldsymbol{k};\tau,\tau_1)\boldsymbol{\phi}_{00j}'(\boldsymbol{k};\tau_1)\,d\tau_1. \ (A17)$$

The higher order terms, $\boldsymbol{\phi}_{0n}'(n\geq 2)$, are expressed in terms of $\boldsymbol{\phi}_{0m}'(m\leq n-1)$ and $\boldsymbol{\psi}_{0m}'(m\leq n-1)$, resulting in a nonlinear dependence on $\boldsymbol{B}$.

The terms on the order of $O(\delta_S)$ have also been obtained as

$$\boldsymbol{\phi}_{1i}^+(\boldsymbol{k};\tau) = -\frac{\partial\Phi_l}{\partial X_j}D_{lm}(\boldsymbol{k})\int_{-\infty}^{\tau}G_{\phi_{im}}'(\boldsymbol{k};\tau,\tau_1)\boldsymbol{\psi}_{0j}'(\boldsymbol{k};\tau_1)\,d\tau_1$$

$$- \int_{-\infty}^{\tau}G_{\phi_{ij}}'(\boldsymbol{k};\tau,\tau_1)\frac{D^*\boldsymbol{\phi}_{00j}'(\boldsymbol{k};\tau_1)}{DT^*}\,d\tau_1$$

$$+ B_j\int_{-\infty}^{\tau}G_{\phi_{il}}'(\boldsymbol{k};\tau,\tau_1)\frac{\partial^*\boldsymbol{\phi}_{00l}'(\boldsymbol{k};\tau_1)}{\partial X_j^*}\,d\tau_1$$

$$- i(\boldsymbol{k}\cdot\boldsymbol{B})\int_{-\infty}^{\tau}G_{\phi_{ij}}'(\boldsymbol{k};\tau,\tau_1)\boldsymbol{\phi}_{1\,j}^{+\,'}(\boldsymbol{k};\tau_1)\,d\tau_1, \quad (A18)$$

with a similar expression for $\boldsymbol{\psi}_1'$. From equations (A17), (A18), and their counterparts for $\boldsymbol{\psi}_{01}'$ and $\boldsymbol{\psi}_1'$, the $O(1)$ and $O(\delta_S)$ solutions may be written in terms of $\boldsymbol{\phi}_{00}'$, $\boldsymbol{\psi}_{00}'$, $G_{\phi_{ij}}'$, and $G_{\psi_{ij}}'$ in addition to $\boldsymbol{B}$ and $\boldsymbol{U}$.

Equation (A15) and its counterpart for $\boldsymbol{\psi}_{00}'$ are not explicitly dependent of the mean field, which is a primary generator of the statistical anisotropy of $\boldsymbol{\phi}'$ and $\boldsymbol{\psi}'$. We thus assume their isotropic correlation functions

$$\frac{\langle Y_i(\boldsymbol{k};\tau)\,Z_j(\boldsymbol{k}';\tau')\rangle}{\delta(\boldsymbol{k}+\boldsymbol{k}')} = D_{ij}(\boldsymbol{k})Q_{YZ}(k;\tau,\tau')$$

$$+ \frac{i}{2}\frac{k_l}{k^2}\epsilon_{ijl}H_{YZ}(k;\tau,\tau'), \quad (A19)$$

$$\langle G_{Y_{ij}}'(\boldsymbol{k};\tau,\tau')\rangle = \delta_{ij}G_{Y_{ij}}(k;\tau,\tau'). \quad (A20)$$

Here, Y and Z represent one of $\boldsymbol{\phi}_{00}'$ and $\boldsymbol{\psi}_{00}'$. For instance, we write

$$\frac{\langle\boldsymbol{\phi}_{00i}'(\boldsymbol{k};\tau)\,\boldsymbol{\psi}_{00j}'(\boldsymbol{k}';\tau')\rangle}{\delta(\boldsymbol{k}+\boldsymbol{k}')} = D_{ij}(\boldsymbol{k})Q_{\phi\psi}(k;\tau,\tau')$$

$$+ \frac{i}{2}\frac{k_l}{k^2}\epsilon_{ijl}H_{\phi\psi}(k;\tau,\tau'). \quad (A21)$$

In using Elsasser's variables, Elsasser's turbulent stress, defined by equation (A9) is expanded as

$$R_{ij}^{(E)} = \langle\boldsymbol{\phi}_{0i}'\boldsymbol{\psi}_{0j}'\rangle + \delta_S\left(\langle\boldsymbol{\phi}_{1i}'\boldsymbol{\psi}_{0j}'\rangle + \langle\boldsymbol{\phi}_{0i}'\boldsymbol{\psi}_{1j}'\rangle\right) + O(\delta_S^2)$$

$$= \langle\boldsymbol{\phi}_{00i}'\boldsymbol{\psi}_{00j}'\rangle + \langle\boldsymbol{\phi}_{01i}'\boldsymbol{\psi}_{00j}'\rangle + \langle\boldsymbol{\phi}_{00i}'\boldsymbol{\psi}_{01j}'\rangle + \cdots$$

$$+ \delta_S\left(\langle\boldsymbol{\phi}_{1i}'\boldsymbol{\psi}_{00j}'\rangle + \langle\boldsymbol{\phi}_{00i}'\boldsymbol{\psi}_{1j}'\rangle + \cdots\right) + O(\delta_S^2). \ (A22)$$

Equations (A14) and (A12) are substituted into equation (A22). With the help of equations (A19) and (A20), one has, after lengthy manipulations,

$$R_{ij}^{(E)} = \frac{2}{3}K^{(E)}\delta_{ij}$$

$$+ \left[\frac{1}{6}\int d\boldsymbol{k}\int_{-\infty}^{\tau}G_\psi(k;\tau,\tau_1)H_{\phi\psi}(k;\tau,\tau_1)\,d\tau_1\right]\epsilon_{ijl}B_l$$

$$+ \left[\frac{1}{6}\int d\boldsymbol{k}\int_{-\infty}^{\tau}G_\phi(k;\tau,\tau_1)H_{\psi\phi}(k;\tau,\tau_1)\,d\tau_1\right]\epsilon_{ijl}B_l$$

$$- \left(\frac{2}{3}\frac{\partial\Psi_j}{\partial x_i} + \frac{1}{15}\frac{\partial\Psi_i}{\partial x_j}\right)$$

$$\times\int d\boldsymbol{k}\int_{-\infty}^{\tau}G_\psi(k;\tau,\tau_1)Q_{\phi\phi}(k;\tau,\tau_1)\,d\tau_1$$

$$- \left(\frac{2}{3}\frac{\partial\Phi_j}{\partial x_i} + \frac{1}{15}\frac{\partial\Phi_i}{\partial x_j}\right)$$

$$\times\int d\boldsymbol{k}\int_{-\infty}^{\tau}G_\phi(k;\tau,\tau_1)Q_{\psi\psi}(k;\tau,\tau_1)\,d\tau_1, \quad (A23)$$

with

$$K^{(E)} = \frac{1}{2}\langle \boldsymbol{\phi}' \cdot \boldsymbol{\psi}' \rangle$$

$$= \int Q_{\phi\psi}(k;\tau,\tau_1)\,dk$$

$$- \frac{1}{2}\int d\boldsymbol{k} \int_{-\infty}^{\tau} G_\psi(k;\tau,\tau_1)\frac{DQ_{\phi\psi}(k;\tau,\tau_1)}{Dt}d\tau_1$$

$$- \frac{1}{2}\int d\boldsymbol{k} \int_{-\infty}^{\tau} G_\phi(k;\tau,\tau_1)\frac{DQ_{\psi\phi}(k;\tau,\tau_1)}{Dt}d\tau_1$$

$$- \frac{1}{4}\left[\int k^{-2}d\boldsymbol{k} \int_{-\infty}^{\tau} G_\psi(k;\tau,\tau_1)\frac{\partial H_{\phi\psi}(k;\tau,\tau_1)}{\partial x_l}d\tau_1\right]B_l$$

$$- \frac{1}{4}\left[\int k^{-2}d\boldsymbol{k} \int_{-\infty}^{\tau} G_\phi(k;\tau,\tau_1)\frac{\partial H_{\psi\phi}(k;\tau,\tau_1)}{\partial x_l}d\tau_1\right]B_l. \tag{A24}$$

We substitute equation (A23) into equations (A10) and (A11), and obtain

$$E_M = \alpha B - \beta J + \gamma \Omega, \tag{A25}$$

where

$$\alpha = \frac{1}{3}\int d\boldsymbol{k} \int_{-\infty}^{\tau} G_+(k,\boldsymbol{x};\tau,\tau_1,t)$$

$$\times [-H_{uu}(k,\boldsymbol{x};\tau,\tau_1,t) + H_{bb}(k,\boldsymbol{x};\tau,\tau_1,t)]\,d\tau_1$$

$$- \frac{1}{3}\int d\boldsymbol{k} \int_{-\infty}^{\tau} G_-(k,\boldsymbol{x};\tau,\tau_1,t)$$

$$\times [-H_{bu}(k,\boldsymbol{x};\tau,\tau_1,t) + H_{ub}(k,\boldsymbol{x};\tau,\tau_1,t)]\,d\tau_1, \tag{A26}$$

$$\beta = \frac{1}{3}\int d\boldsymbol{k} \int_{-\infty}^{\tau} G_+(k,\boldsymbol{x};\tau,\tau_1,t)$$

$$\times [Q_{uu}(k,\boldsymbol{x};\tau,\tau_1,t) + Q_{bb}(k,\boldsymbol{x};\tau,\tau_1,t)]\,d\tau_1$$

$$- \frac{1}{3}\int d\boldsymbol{k} \int_{-\infty}^{\tau} G_-(k,\boldsymbol{x};\tau,\tau_1,t)$$

$$\times [Q_{ub}(k,\boldsymbol{x};\tau,\tau_1,t) + Q_{bu}(k,\boldsymbol{x};\tau,\tau_1,t)]\,d\tau_1, \tag{A27}$$

$$\gamma = \frac{1}{3}\int d\boldsymbol{k} \int_{-\infty}^{\tau} G_+(k,\boldsymbol{x};\tau,\tau_1,t)$$

$$\times [Q_{ub}(k,\boldsymbol{x};\tau,\tau_1,t) + Q_{bu}(k,\boldsymbol{x};\tau,\tau_1,t)]\,d\tau_1$$

$$- \frac{1}{3}\int d\boldsymbol{k} \int_{-\infty}^{\tau} G_-(k,\boldsymbol{x};\tau,\tau_1,t)$$

$$\times [Q_{uu}(k,\boldsymbol{x};\tau,\tau_1,t) + Q_{bb}(k,\boldsymbol{x};\tau,\tau_1,t)]\,d\tau_1, \tag{A28}$$

and $G_+ = (G_\phi + G_\psi)/2$, $G_- = (G_\phi - G_\psi)/2$, with the dependence on slow variables explicitly shown through $\boldsymbol{x}$ and t in this equation. The term (A28) shows the cross-helicity dynamo mechanism.

A one-point modeling is deduced from equations (A26)–(A28). Integrals of $Q_{YZ}(k;\tau,\tau')$ and $H_{YZ}(k;\tau,\tau')$ over k give the turbulent MHD energy, $K = \langle(\boldsymbol{u}'^2 + \boldsymbol{b}'^2)/2\rangle$, the turbulent cross helicity, $W = \langle \boldsymbol{u}' \cdot \boldsymbol{b}'\rangle$, and the turbulent residual helicity $H = \langle -\boldsymbol{u}' \cdot \boldsymbol{\omega}' + \boldsymbol{b}' \cdot \boldsymbol{j}'\rangle$. The integral of the Green's function provides

$$\tau_M(k) = \int_{-\infty}^{\tau} G_+(k,\boldsymbol{x};\tau,\tau_1,t)\,d\tau_1, \tag{A29}$$

which expresses the time scale associated with the spatial length, k^{-1}. For a representative wave number, $\tau_M(k)$ provides the autocorrelation time, τ_c. The magnetic perturbation contributes to the magnetic diffusivity, as explicitly shown in a nonlinear simulation (see, e.g., Müller, Carti 2002). Nevertheless, by introducing the property of the 3D MHD turbulence, which relates the magnetic fluctuation intensity to the velocity turbulence intensity, β can be expressed in terms of the kinematic magnetic diffusivity, $\beta = C_\beta \langle \boldsymbol{u}'^2\rangle\tau_c$ (Diamond et al. 2004; Vainshtein, Kitchatinov 1983; Montgomery, Chen 1984). Thus, the integrals in equations (A26)–(A28) are in proportion to $\tau_c H$, $\tau_c K_K$, and $\tau_c W$, respectively ($K_K = \langle \boldsymbol{u}'^2/2\rangle$). Thus, by introducing numerical coefficients C_α, C_β, and C_γ, we write $\alpha = C_\alpha\tau_c H$, $\beta = C_\beta\tau_c K_K$, and $\gamma = C_\gamma\tau_c W$. Numerical coefficients C_α, C_β, and C_γ have been determined by comparing with direct numerical simulations.

Similarly, the Reynolds stress, R_{ij}, is written as

$$R_{ij} = \frac{2}{3}K_R\delta_{ij} - \nu_T S_{ij} + \nu_M M_{ij}, \tag{A30}$$

where K_R is defined by $K_R = \langle \boldsymbol{u}'^2 - \boldsymbol{b}'^2\rangle/2 = \int Q_K(k;\tau,\tau')dk - \int Q_M(k;\tau,\tau')dk$, and $M_{ij} = \partial B_j/\partial x_i + \partial B_i/\partial x_j$. Detailed discussion on ν_T and ν_M was also developed in (Yoshizawa 1990). The key is that the terms β and ν_T are induced by the fluctuation energy intensity, while the terms γ and ν_M are caused by the cross-helicity of the MHD turbulence, and that the correlation time (integral of Green's function) is taken to be common for these four quantities. Thus, an evaluation has been given,

$$\frac{\nu_M}{\nu_T} \simeq \frac{\gamma}{\beta}. \tag{A31}$$

[See: Yoshizawa et al. (2004). Note that other modeling may provide a relation with a different magnitude of the ratio, e.g., $\nu_M/\nu_T \simeq C_r \gamma/\beta$. Nevertheless, the difference in the ratio C_r does not cause a qualitative change in the conclusion of this analysis.] The term $\nu_M M_{ij}$ in R_{ij} represents the drive of rotation owing to the magnetic field in the presence of the cross-helicity dynamo process.

Appendix 3.   Solution Which is Regular at the Center

The main interest of this article is to understand the toroidal structure in a shelluar domain, such as a convective zone. Recently, a proposal for the magnetic field in the central core of the Sun has been given (Gough, McIntyre 1998). The domain where the magnetic field is generated is considered to include the center. Then the toroidal structure, if it exists, is singular at the center. In such a case, the toroidal solution is given as

$$B_\zeta(r, \theta) = a_1 j_1(y) P_1^{(1)}(\cos \theta) + \cdots \qquad \text{(A32)}$$

$$B_\theta(r, \theta) = -a_1 \left[\frac{2 j_1(y)}{y} - j_2(y) \right] P_1^{(1)}(\cos \theta) + \cdots \qquad \text{(A33)}$$

$$B_r(r, \theta) = a_1 \frac{j_1(y)}{y} \left[\frac{2 \cos \theta}{\sin \theta} P_1^{(1)}(\cos \theta) - P_1^{(2)}(\cos \theta) \right] + \cdots \qquad \text{(A34)}$$

where $+ \cdots$ indicates the higher harmonics. The eigenvalue condition is given at a radius where the radial magnetic field vanishes.

This solution has a dipole component, as in Gough and McIntyre (1998), but has a topology of a torus. Because it is force free, the global magnetic energy associated with the mean magnetic field takes a (local) minimum. Therefore it is more stable compared with the solution with a pure dipole magnetic field.

References

Barnes, J. R., James, D. J., & Cameron, A. C. 2004, MNRAS, 352, 589

Blackman, E. G. 2000, ApJ, 529, 138

Blackman, E. G., & Chou, T. 1997 ApJ, 489, L95

Busse, F. H. 1994, Chaos, 4, 123

Covas, E., Tavakol, R., & Moss, D. 2001, A&A, 371, 718

Diamond, P. H., Hughes, D. W., & Kim, E.-J. 2004, in The Fluid Mechanics of Astrophysics and Geophysics, ed. A. M. Soward, C. A. Jones, D. W. Hughes, & N. O. Weiss (London: CRC Press), 12, 145

Donati, J.-F., et al. 2003, MNRAS, 345, 1145

Fan, Y., & Gong, D. 2000, Solar Phys., 192, 141

Gough, D. O., & McIntyre, M. E. 1998, Nature, 394, 755

Gruzinov, A. V., & Diamond, P. H. 1994, Phys. Rev. Lett., 72, 1651

Itoh, S.-I., Itoh, K., Yoshizawa, A., & Yokoi, N. 2005, ApJ, 618, 1044

Itoh, S.-I., Itoh, K., Zushi, H., & Fukuyama, A. 1998, Plasma Phys. Control. Fusion, 40, 879

Kitchatinov, L. L., Rüdiger, G., & Küeker, M. 1994, A&A, 292, 125

Krause, F., & Raedler, K. H. 1980, Mean-Field Electrodynamics and Dynamo Theory (Oxford: Pergamon Press)

Lang, K. R. 2001, The Cambridge Encyclopedia of the Sun (Cambridge: Cambridge University Press)

Moffatt, H. K. 1978, Magnetic field generation in electrically conducting fluids (Cambridge: Cambridge University Press)

Montgomery, D., & Chen, H. 1984, Plasma Phys. Control. Fusion, 26, 1199

Müller, W.-C., & Carati, D. 2002, Phys. Plasmas, 9, 824

O'Neal, D., Neff, J. E., & Saar, S. H. 1998, ApJ, 507, 919

Parker, E. N. 1993, ApJ, 408, 707

Priest, E. R. 1982, Solar Magneto-hydrodynamics (Dordrecht: Reidel)

Rüdiger, G., & Brandenburg, A. 1995, A&A, 296, 557

Rüdiger, G., & Hollerbach, R. 2004, The Magnetic Universe (Weinheim: Wiley-VCH)

Rüdiger, G., & Kitchatinov, L. L. 1990, A&A, 236, 503

Shibahashi, H. 2002, J. Plasma Fusion Res., 78, 497

Shibahashi, H. 2004, in Proc. IAU Symp. No. 223, 23

Sweet, P. A. 1950, MNRAS, 110, 548

Taylor, J. B. 1986, Rev. Mod. Phys., 58, 741

Vainshtein, S. I., & Kitchatinov, L. L. 1983, Geophys. Astrophys. Fluid Dyn., 24, 273

Yoshimura, H. 1972, ApJ, 178, 863

Yoshimura, H. 1981, ApJ, 247, 1102

Yoshizawa, A. 1990, Phys. Fluids B, 2, 1589

Yoshizawa, A., Itoh, S.-I., & Itoh, K. 2003, Plasma Phys. Control. Fusion, 45, 321

Yoshizawa, A, Itoh, S.-I., Itoh, K., & Yokoi, N. 2004, Plasma Phys. Control. Fusion, 46, R25

Yoshizawa, A., Kato, H., & Yokoi, N. 2000, ApJ, 537, 1039